CRYSTAL GROWTH & DESIGN

ARTICLE

pubs.acs.org/crystal

Sulfonamide Molecular Crystals: Thermodynamic and Structural Aspects

German L. Perlovich,*[,†] Alex M. Ryzhakov,[†] Valery V. Tkachev,[‡] and Lars Kr. Hansen[§]

[†]Institute of Solution Chemistry, Russian Academy of Sciences, 153045 Ivanovo, Russia

[‡]Laboratory of Structural Chemistry, Institute of Problems of Chemical Physics, Russian Academy of Sciences, 142432, Chernogolovka, Russia

[§]University of Tromsø, Institute of Chemistry, Breivika, N-9037 Tromsø, Norway

Supporting Information

ABSTRACT: The crystal structures of three sulfonamides with the structures C_6H_5-SO_2NH-C_6H_5, C_6H_5-SO_2NH-C_6H_4-R (R = 4-NO_2), 4-NH_2-C_6H_4-SO_2NH-C_6H_4-R (R = 4-NO_2; 4-CN) have been determined by X-ray diffraction. On the basis of our previous data and the obtained results, comparative analysis of crystal properties was performed: molecular conformational states, packing architecture, and hydrogen bond networks using graph set notations. Conformational flexibility of the bridge connecting two phenyl rings was studied and described by a correlation equation. Hydrogen bonds were grouped according to the frequency of hydrogen bond appearance within the definite graph set assignment. The strength of the hydrogen bonds was evaluated. The influence of various molecular fragments on crystal lattice energy was analyzed. A correlation between melting points and fragmental molecular interactions in the crystal lattices was obtained. The thermodynamic aspects of the sulfonamide sublimation were studied by investigating the temperature dependence of vapor pressure using the transpiration method. A correlation between the Gibbs energy of the sublimation process and molecular H-bond acceptor factors was found. In addition, a regression equation was derived for describing the correlation between the sublimation entropy terms and crystal density data calculated from X-ray diffraction results. These dependencies allow us to predict sublimation thermodynamic parameters not knowing more than the molecular formula and crystal density.

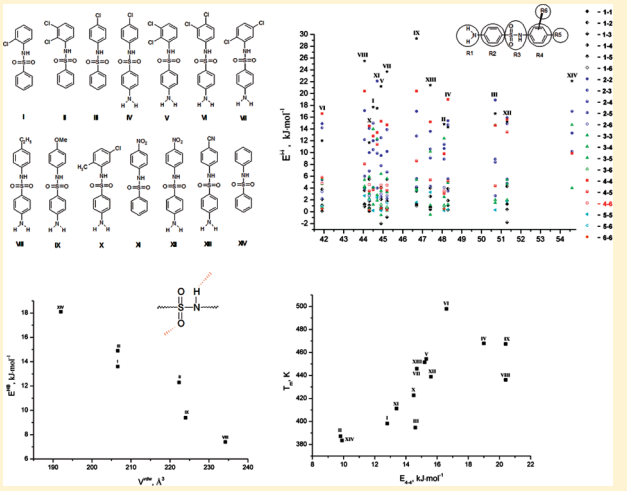

INTRODUCTION

Sulfonamides (SAs) are drugs extensively used for treating certain infections caused by Gram-positive and Gram-negative microorganisms, some fungi, and certain protozoa. Although the extensive use of antibiotics has diminished the usefulness of SAs, they still occupy a relatively small but important place in the therapeutic resources of physicians.[1] Usually the compounds under consideration are poorly soluble in aqueous mediums, and this fact is an essential obstacle for the drug delivery. Therefore, the molecular structure design (without disturbing the pharmacological site), giving an opportunity to obtain the minimal values of crystal lattice energies, is an important task for pharmaceutics and crystal engineering. Sulfonamide molecules in crystals are inclined to create hydrogen bond networks with complicated topological structures. Therefore, it is sometimes difficult to estimate crystal lattice energy on the basis of even crystal structure data.

A careful analysis of published SA crystal lattice structures has been carried out by Adsmond and Grant.[2] In this work, special attention was paid to the hydrogen bond networks characterization and systematization by using graph set notations. Moreover, the authors tried to describe donor and acceptor affinities of atoms in the molecules studied on the basis of the statistical analysis of hydrogen bonds of solvated and nonsolvated crystals. Furthermore, this class of substances attracted the researchers' attention from the point of view of the fundamental aspects of studying supramolecular aggregation in a cognate series of substituted sulfonamides. Kelly et al.[3] investigated the impact of iodine and nitro groups at different positions of the aryl ring on a wide range of different but competitive supramolecular interactions.

Understanding the structural conformation of sulfonamides is vital for drug design, since the sulfonamide group is an extremely important biological functional group and determines biological

Received: September 20, 2010
Revised: January 5, 2011
Published: February 10, 2011

dx.doi.org/10.1021/cg1012389 | *Cryst. Growth Des.* 2011, 11, 1067–1081

Scheme 1

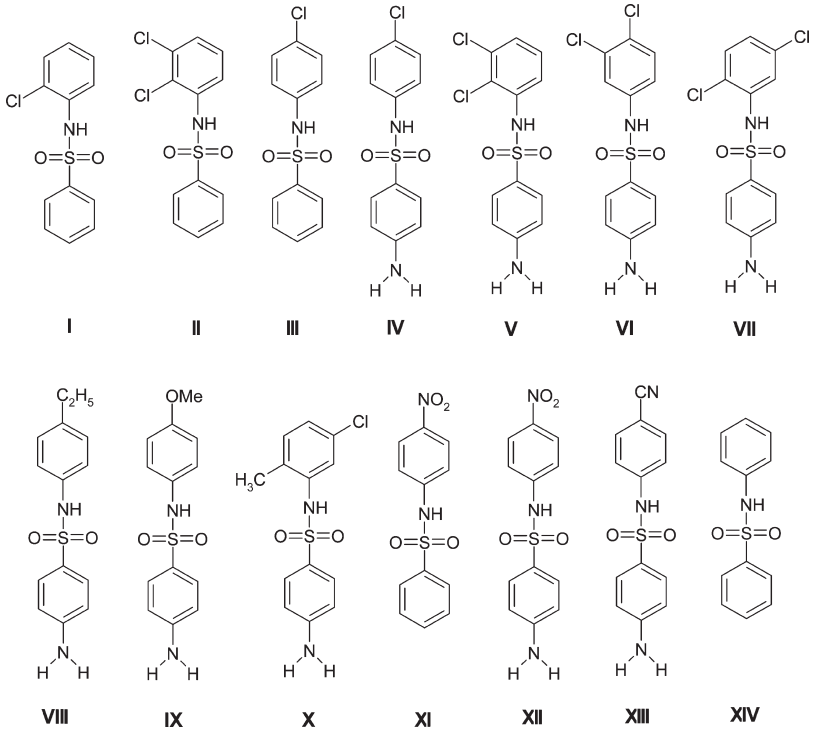

activity. Several works were devoted to the analysis of conformational states of sulfonamide molecules in crystals. It is essential to mention the paper of Parkin et al.,[4] who have carried out comparative analysis of torsion angles of SA small molecules on the basis of CDS.[5] This work did not consider the phenyl fragments connected with the sulfonamide bridge. Nevertheless, the values, describing average statistical molecular conformations, coincide with the torsion angles obtained by us in this work. Adsmond and Grant[2] analyzed three torsion angles characterizing the sulfonamide bridge mobility and concluded that sulfonamides in the amide tautomer have a large degree of conformational mobility due to the three single bonds C−S−N−C joining the two ends of the molecule. Moreover, all angles correspond to the extended Huckel (EHMO) calculations, carried out by Kalman et al.[6] The exception connected with sulfamoxolez was explained by hydrogen bond networks with motif $R_2^2(16)$. The recent paper[7] has used the results of the calculations on sulfonamide conformations to explain the increase in the activity of a particular potential drug compound over another. Although their assumptions may be correct, the calculations as described use information from the work of Bindal et al.[8] that has since been shown to contain erroneous assumptions about N-methylmethanesulfonamide in the solid state.[9]

Our previous works[10−12] studied the structures, packing architecture, topology of hydrogen bond networks, sublimation, solubility, and solvation characteristics of the 10 sulfonamides. As a continuation of the study, this work focuses on the comparative analysis of the published compounds *N*-(2-chlorophenyl)-benzenesulfonamide (**I**), *N*-(2,3-dichlorophenyl)-benzene-sulfonamide (**II**), *N*-(4-chlorophenyl)-benzene-sulfonamide (**III**), 4-amino-*N*-(4-chlorophenyl)-benzene-sulfonamide (**IV**), 4-amino-*N*-(2,3-dichlorophenyl)-benzene-sulfonamide (**V**), 4-amino-*N*-(3,4-dichlorophenyl)-benzene-sulfonamide (**VI**), 4-amino-*N*-(2,5-dichlorophenyl)-benzene-sulfonamide (**VII**), 4-amino-*N*-(4-ethylphenyl)-benzene-sulfonamide (**VIII**), 4-amino-*N*-(4-methoxyphenyl)-benzene-sulfonamide (**IX**), and 4-amino-*N*-(5-chloro-2-methylphenyl)-benzene-sulfonamide (**X**) with new ones: *N*-(4-nitrophenyl)-benzene-sulfonamide (**XI**); 4-amino-*N*-(4-nitrophenyl)-benzene-sulfonamide (**XII**); 4-amino-*N*-(4-cyanophenyl)-benzene-sulfonamide (**XIII**); *N*-phenyl-benzene-sulfonamide (**XIV**) (Scheme 1).

The choice of the compounds was dictated by the following aims. First, we aimed to analyze the influence of substituent nature and molecular topology on the molecule conformational state, the formation of crystal lattice architecture, and hydrogen bond networks. Second, we planned to study the thermodynamic and thermophysical properties of the crystals and find out the relationship between the noted parameters and crystal structure.

EXPERIMENTAL SECTION

Compounds and Solvents. The chemical synthesis of SAs (**XI**−**XIII**) has been performed according to the procedures described earlier[10−12] by the reaction of a substituted aromatic amine with 4-acetylaminobenzenesulfonyl chloride in dry pyridine, followed by hydrolytic deacetylation in alkaline aqueous medium (∼1 M NaOH) and precipitation of the end product by acidification (∼1 M HCl) to pH 5. The compounds were carefully purified by recrystallizing from water−ethanol solution. The precipitate was filtered and dried at room temperature under a vacuum until the mass of compounds remained constant. The outlined procedure was repeated several times and the product was checked by NMR after each recrystallization step until the proton NMR signal correspondence to the purity of the compound was over 99%. *N*-Phenyl-benzene-sulfonamide was obtained from Sigma Chemical Co. (USA).

Single crystals of the title compounds were grown from a water−ethanol solution (initial composition 20:1 v/v) by the vapor diffusion of ethanol vapor into pure water.[13]

dx.doi.org/10.1021/cg1012389 |*Cryst. Growth Des.* 2011, 11, 1067–1081

Table 1. Crystal Lattice Parameters of the Substances under Investigation[a]

	XI	XII	XIII	XIV
crystal system	monoclinic	orthorhombic	monoclinic	tetragonal
space group	$P2_1/c$	*Pbca*	$C2/c$	$P4_32_12$
crystal size, mm	0.26 × 0.2 × 0.14	0.35 × 0.25 × 0.02	0.35 × 0.25 × 0.15	0.40 × 0.20 × 0.05
a, Å	12.7510(19)	5.7526(11)	26.764(6)	8.8551(19)
b, Å	8.4820(17)	15.465(3)	24.756(5)	8.8551(19)
c, Å	11.5790(12)	30.087(6)	8.0027(17)	30.282(7)
α, °	90.00	90.00	90.00	90.00
β, °	99.450(2)	90.00	100.543(4)	90.00
γ, °	90.00	90.00	90.00	90.00
volume, Å^3	1235.3(3)	2676.7(9)	5212.9(19)	2374.5(9)
Z	4	8	16	8
D_{calc}, g·cm^{-3}	1.496	1.455	1.393	1.305
radiation	Mo K$_\alpha$	Mo K$_\alpha$	Mo K$_\alpha$	Mo K$_\alpha$
T, K	293(2)	293.1	293.1	293.1
μ, mm^{-1}	0.274	0.259	0.062	0.26
Data collection				
measured reflections	2553	10062	14665	5734
independent reflections	1916	3591	6789	3105
independent reflections with >2$\sigma(I)$	1240	1122	3085	2798
R_{int}	0.0283	0.063	0.037	0.054
θ_{max}, °	25.0	30.70	30.72	30.6
Refinement				
refinement on	F^2	F^2	F^2	F^2
$R[F^2 > 2\sigma(F^2)]$	0.0389	0.054	0.0626	0.0615
$\omega R(F^2)$	0.0881	0.069	0.067	0.0537
S	1.002	1.15	1.062	1.135
reflections	1916	1605	3160	2851
parameters	177	198	377	189
$(\Delta/\sigma)_{max}$	0.000	0.031	0.0048	0.0143
$\Delta\rho_{max}$, e·Å^{-3}	0.189	0.39	0.27	0.69
$\Delta\rho_{min}$, e·Å^{-3}	−0.225	−0.39	−0.40	−0.68

[a] Standard deviations are presented in parentheses.

Methods. *X-ray Diffraction Experiments.* Single-crystal X-ray measurements were carried out using a Nonius CAD-4 diffractometer with graphite-monochromated Mo K$_\alpha$ radiation (λ = 0.71069 Å). Intensity data were collected at 25 °C by means of a ω-2θ scanning procedure. The crystal structures were solved using direct methods and refined by means of a full-matrix least-squares procedure. CAD-4[14] was applied for data collection, data reduction, and cell refinement. Programs SHELXS-97 and SHELXL-97[15] were used to solve and to refine structures, respectively.

Sublimation Experiments. Sublimation experiments were carried out by the transpiration method as was described elsewhere.[16] In brief: a stream of an inert gas passes above the sample at a constant temperature and at a known slow constant flow rate in order to achieve saturation of the carrier gas with the vapor of the substance under investigation. The vapor is condensed at some point downstream, and the mass of sublimate and its purity are determined. The vapor pressure over the sample at this temperature can be calculated by the amount of the sublimated sample and the volume of the inert gas used.

The equipment was calibrated using benzoic acid. The standard value of sublimation enthalpy obtained here was $\Delta H^0_{sub} = 90.5 \pm 0.3$ J·mol^{-1}. This is in good agreement with the value recommended by IUPAC of ΔH^0_{sub} = 89.7 ± 0.5 J·mol^{-1}.[17] The saturated vapor pressures were measured five times at each temperature with the standard deviation being within 3−5%. Because the saturated vapor pressure of the investigated compounds is low, it may be assumed that the heat capacity change of the vapor with temperature is so small that it can be neglected. The experimentally determined vapor pressure data may be described in (ln P; 1/*T*) coordinates in the following way:

$$\ln(p) = A + B/T \quad (1)$$

The value of the sublimation enthalpy is calculated by the Clausius−Clapeyron equation:

$$\Delta H^T_{sub} = RT^2 \cdot \partial(\ln P)/\partial(T) \quad (2)$$

whereas the sublimation entropy at the given temperature *T* was calculated from the following relation:

$$\Delta S^T_{sub} = (\Delta H^T_{sub} - \Delta G^T_{sub})/T \quad (3)$$

with $\Delta G^T_{sub} = -RT\ln(P/P_0)$, where P_0 is the standard pressure of 1.013 × 10^5 Pa.

For experimental reasons sublimation data are obtained at elevated temperatures. However, in comparison with effusion methods, the temperatures are much lower, which makes extrapolation to room conditions easier. In order to further improve the extrapolation to room conditions, we estimated the heat capacities ($C^{298}_{p,cr}$-value) of the crystals using the additive scheme proposed by Chickos et al.[18] Heat capacity

dx.doi.org/10.1021/cg1012389 |*Cryst. Growth Des.* 2011, 11, 1067–1081

was introduced as a correction for the recalculation of the sublimation enthalpy ΔH^{T}_{sub}-value at 298 K (ΔH^{298}_{sub}-value), according to the equation[18] (the procedure of $C^{298}_{p,cr}$-value calculation is presented in Table 7):

$$\Delta H^{298}_{sub} = \Delta H^{T}_{sub} + \Delta H_{cor} = \Delta H^{T}_{sub} + (0.75 + 0.15C^{298}_{p,cr})(T - 298.15) \quad (4)$$

Differential Scanning Calorimetry. Differential scanning calorimetry (DSC) was carried out using a Perkin-Elmer Pyris 1 DSC differential scanning calorimeter (Perkin-Elmer Analytical Instruments, Norwalk, Connecticut, USA) with Pyris software for Windows NT. DSC runs were performed in an atmosphere of flowing (20 mL·min^{-1}) dry helium gas of high purity 99.996% using standard aluminum sample pans and a heating rate of 10 K·min^{-1}. The accuracy of weight measurements was ±0.005 mg. The DSC was calibrated with an indium sample from Perkin-Elmer (P/N 0319-0033). The value determined for the enthalpy of fusion corresponded to 28.48 J·g^{-1} (reference value 28.45 J·g^{-1}). The melting point was 156.5 ± 0.1 °C

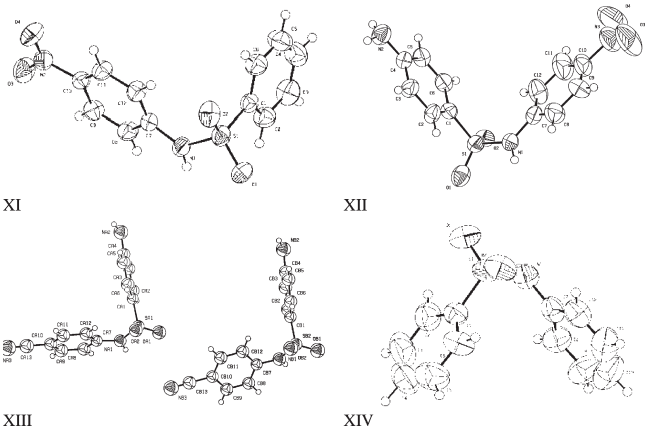

Figure 1. A view of molecules **IX**−**IV** with atomic numbering.

(n = 10). The enthalpy of fusion at 298 K was calculated by the following equation:

$$\Delta H^{298}_{fus} = \Delta H_{fus} - \Delta S_{fus}(T_m - 298.15) \quad (5)$$

where the difference between the heat capacities of the melt and solid states was approximated by the fusion entropy (as an upper estimate). This approach was used by Dannenfelser and Yalkowsky.[19]

The enthalpy of vaporization was calculated as

$$\Delta H^{298}_{vap} = \Delta H^{298}_{sub} - \Delta H^{298}_{fus} \quad (6)$$

Calculation Procedure. The free molecular volume in the crystal lattice was estimated on the basis of the X-ray diffraction data and van der Waals molecular volume (V^{vdw}), calculated by GEPOL:[20]

$$V^{free} = (V_{cell} - ZV^{vdw})/Z \quad (7)$$

where V_{cell} is the volume of the unit cell, and Z is the number of molecules in the unit cell.

All descriptors were calculated by the program package HYBOTPLUS (version of 2003 year) in Windows.[21]

Nonbonded van der Waals interactions of crystal lattice energy were calculated as a sum of atom−atom interactions with the help of Gavezzotti et al.[28] force field and cutoff radius 16 Å. The hydrogen bonding energy was calculated with the help of Mayo et al.[24] force field:

$$E^{HB} = D_{HB}[5(R_{hb}/R_{DA})^{12} - 6(R_{hb}/R_{DA})^{10}] \cos^4(\theta_{DHA}) \quad (8)$$

where D_{HB} = 39.7 kJ·mol^{-1} is a depth of potential well of pair potential at the creation of the hydrogen bond of H_2O dimer; R_{hb} = 2.75 Å; R_{DA}, θ_{DHA} are the distance and angle between donor and acceptors atoms.

RESULTS AND DISCUSSION

Crystal Structure Analysis. *Molecular Conformational Analysis.* The results of the X-ray diffraction experiments are presented in Table 1.

In order to characterize the conformational states of the molecules, Figure 1 shows the view of representative molecule **XI** with atomic numbering. This numbering was used for all

Table 2. Some Parameters (°) Describing Molecular Conformational States in the Crystal Lattices

	∠C2−C1−S1−N1 (τ_1)	∠C7−N1−S1−C1 (τ_2)	∠C12−C7−N1−S1 (τ_3)	∠Ph1−Ph2
I[a]	−108.5(2)	−67.7(2)	−68.3(2)	49.14(9)
II[a]	−106.8(4)	−68.6(4)	−63.8(4)	54.8(2)
III[a]	−83.4(4)	−56.1(3)	−71.1(4)	54.4(2)
IV(A)[b]	−71.7(4)	−54.4(4)	−36.4(5)	80.7(1)
IV(B)[b]	−74.4(4)	−52.1(4)	−79.1(4)	60.5(2)
V(A)[b]	−64.8(2)	−55.3(2)	−28.1(2)	81.56(6)
V(B)[b]	−75.6(2)	−57.0(2)	−43.0(2)	79.11(7)
VI(A)[b]	−66.7(9)	−58.2(9)	−33(1)	84.7(3)
VI(B)[b]	−71.1(9)	−52.7(9)	−80(1)	60.7(4)
VII[b]	−72.3(3)	−52.4(3)	−65.9(3)	64.9(1)
VIII[c]	−75.0(2)	−66.2(2)	−72.7(2)	64.4(6)
IX[c]	−78.0(2)	−68.0(2)	−77.0(2)	60.7(7)
X[c]	−73.4(2)	−54.4(2)	−62.1(2)	67.61(8)
XI	−64.6(3)	−70.8(3)	−31.2(4)	91.2(2)
XII	−72.8(4)	−63.5(4)	−22.3(6)	89.5(4)
XIII(A)	−59.0(3)	−62.8(3)	−21.4(5)	86.7(6)
XIII(B)	−43.4(4)	−81.8(4)	25.7(5)	83.1(7)
XIV	−85.3(4)	−57.7(3)	−67.3(6)	64.1(4)

[a] Ref 10. [b] Ref 11. [c] Ref 12.

dx.doi.org/10.1021/cg1012389 |*Cryst. Growth Des.* 2011, 11, 1067–1081

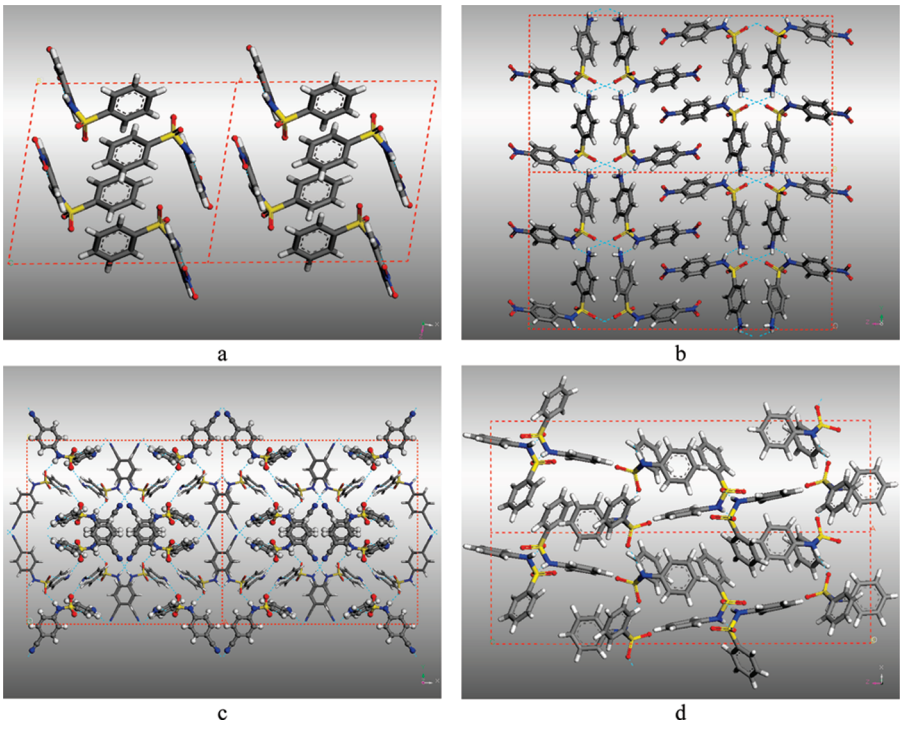

Figure 2. Molecular packing architectures of (**XI**) (a), (**XII**) (b), (**XIII**) (c), and (**XIV**) (d) crystal lattices (stick corresponds to molecule A, whereas the stick and ball correspond to molecule B).

compounds under investigation. The compound XIII has two molecules (A and B) in the asymmetric unit of the crystal lattice. On the basis of the presented numbering, it is possible to carry out the comparative analysis of conformational states of molecules **I**−**XIV**. The results are summarized in Table 2.

The molecular packing architectures of the four new substances under investigation are presented in Figure 2.

The conformational states of the molecules under investigation depend on the mobility of the bridge, connecting two phenyl rings. In order to describe the conformational state we have chosen three parameters (analogous to Parkin et al.[4]): the angle between the SO_2-group and the phenyl motif Ph1 (C1−C2−C3−C4−C5−C6) ∠C2−C1−S1−N1 (τ_1); the angle ∠C7−N1−S1−C1 (τ_2), describing the S1−N1 bond mobility and the torsion angle ∠C12−C7−N1−S1 (τ_3), which characterizes the location of the second phenyl ring Ph2 (C7−C8−C9−C10−C11−C12) relative to the NH-group. Moreover, we introduced an angle between the two phenyl rings ∠Ph1−Ph2 (the acute angle between the least-squares planes through the two phenyl rings) (Table 2). In addition to the noted angles we introduced an angle, equal to the sum of the dihedral angles ($\Sigma\tau_i = \tau_1 + \tau_2 + \tau_3$), which describes the integral flexibility of the bridge connecting the phenyl rings.

Molecular conformational state in crystal lattice depends on different factors: molecular topology, ability of atoms to take part in donor−acceptor interactions, presence of hydrogen bonds and their topological structure, availability of $\pi-\pi$ interactions and interactions with charge transfer, etc. Therefore, it is difficult to pick out only one descriptor to describe both the molecular conformational state and the physicochemical properties of crystal. In our previous work[12] we used the V^{free}/V^{vdw}-parameter, characterizing molecular packing density in crystal. In this work, we have tried to find out a correlation of the studied properties

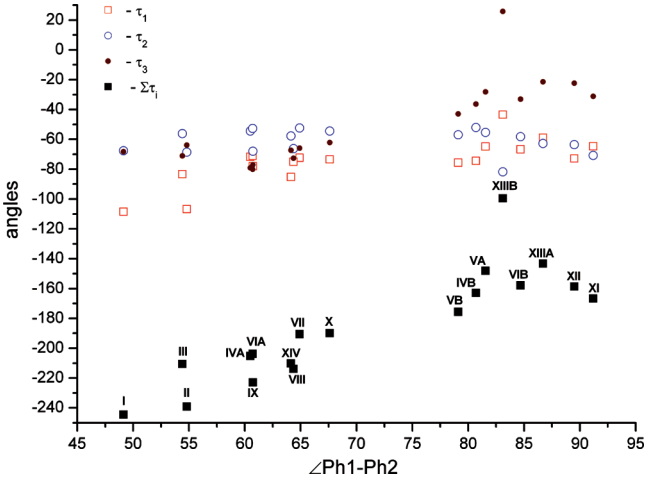

Figure 3. Dependencies of the torsion angles (τ_1, τ_2, τ_3) characterizing mobility of the bridge connecting the two phenyl motives and $\Sigma\tau_i$ versus the angle between the phenyl fragments.

with HYBOT descriptors.[21] It should be noted that primordially 32 descriptors were tested to find suitable correlations; they take into account a whole diversity of interactions in the crystals mentioned before. The τ_1, τ_2, and τ_3 values versus the angle between the phenyl fragments of studied SA are presented in Figure 3. It should be mentioned that all compounds under consideration break up into two conformational populations (if the angles between the phenyl rings are taken into consideration). The first one includes SA with angles 47° < ∠Ph1−Ph2 < 67°, whereas the second one − SA with angles: 77° < ∠Ph1−Ph2 < 92°. It is not difficult to see that no correlation between the introduced dihedral angles (τ_1, τ_2, τ_3) and the angles between the

dx.doi.org/10.1021/cg1012389 |*Cryst. Growth Des.* 2011, 11, 1067–1081

phenyl rings is observed. For the integral angle ($\Sigma\tau_i$) we observed the following regularity. For the low-angle conformational population, the angle between the phenyl rings increases with decreasing the integral mobility of the bridge. For the large-angle populations, a dependence with the extreme value for the compound **XIIIB** is observed.

As the number of the studied SAs was restricted by 14, we declined to build multivariate correlation models due to their low statistical significance. We collected as a dependent variable the integral angle ($\Sigma\tau_i$) describing the bridge flexibility. As independent variables, physicochemical descriptors of program HYBOT[21] were chosen. The analysis of the 32 descriptors showed that the integral angle can be best described by the descriptor indicating the sum of H-bond acceptor factors (ΣC_a)

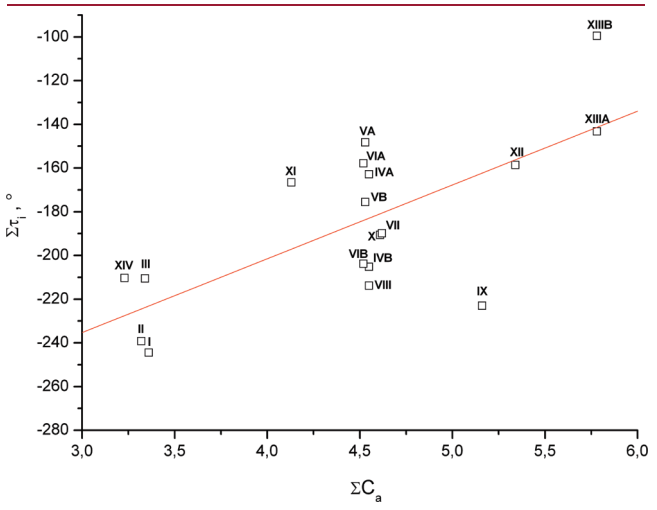

Figure 4. Plot of the integral angle ($\Sigma\tau_i$) versus the sum of H-bond acceptor factors (ΣC_a).

of the molecule. The H-bond atom acceptor factor (C_a) has been obtained from the database including Gibbs energies (binding constants) of complexation processes between different compounds in CCl_4 solution. The results of the analysis are presented in Figure 4. It is not difficult to see that the following regularity is observed: while the H-bond acceptor factor increases, the integral mobility of the bridge decreases. In other words, donor−acceptor interactions and hydrogen bonding in the crystals lead to a reduction of the bridge mobility.

Hydrogen Bond Networks Analysis. The considered compounds create hydrogen bonds in the crystal lattices. Moreover, the number of hydrogen bonds per molecule varies essentially and depends on the molecular topology and presence of hydrogen bond centers. Furthermore, the hydrogen bonds in the crystals create hydrogen bond networks with different topological structures, which influence the thermodynamic and thermophysical properties: particularly the crystal lattice energy, and, as a consequence, the solubility processes. Therefore, the next step included analyzing the hydrogen bond network topology using the graph set notation terminology introduced by Etter[22] and revised by Bernstein.[23] The comparative characteristics of the hydrogen bond geometric parameters, graph set assignments for the two levels are summarized in Table 3. The graph set notations mentioned in Table 3 are illustrated in Table 4.

In order to compare the strength of hydrogen bonds created in the SA crystals, we calculated the hydrogen bond energies (E^{HB}) according to Mayo et al.[24] Therefore, the wide spectrum of geometric characteristics, describing the hydrogen bonds, was reduced to comparable values. For the analysis, we collected only the diagonal elements of graph set assignments matrix (first level). The hydrogen bonds were grouped in accordance with the frequency of their appearance (within the graph set assignment) for the chosen compounds (Table 5). As it follows from Table 5, the graph set notations can be arranged (according to the frequency of appearance in the studied crystals) in the following way: C(8)-1 (type 1) (24 times) > D-2 (10) > C(8)-2 (7) >C(4)-1

Table 3. Hydrogen Bond Geometry and Graph Set Notations of the Molecules Studied

XI	D−H(X)···A(Y)[a,b]	D−H[Å]	H···A[Å]	D···A[Å]	D−H···A[deg]		a
a	N1−H1(A)···O2^{i}(A)	0.84(3)	2.156(3)	2.992(4)	173(3)	a	C(8)(type 3)

XII	D−H(X)···A(Y)[c]	D−H	H···A	D···A	D−H···A	a	b	c	d
a	N2−H2B(A)···O2^{i}(A)	0.793	2.482	3.190	149.3	a	C(8)(type 1)		
b	N2−H2A(A)···O1 ^{ii}(A)	0.888	2.635	3.075	111.7	b	$R_4^4(22)$	C(8)(type 1)	
c	N2−H2A(A)···O1 ^{iii}(A)	0.888	2.616	3.195	123.7	c	$R_4^4(22)$	$R_3^3(18)$	C(8)(type 1)
d	N1−H1(A)···N2^{iv}(A)	0.889	2.204	2.988	146.9	f	$R_4^4(22)$	$R_4^4(22)$	C(8)[$R_2^2(6)$]	C(8)(type 2)

XIII	D−H(X)···A(Y)[d]	D−H	H···A	D···A	D−H···A	a	b	c	d	e	f
a	Nb1−Hb1(B)···Oa1^{i}(A)	0.889	2.028	2.841	151.4	a	D(type 1)				
b	Na2−Ha2B(A)···Ob1 ^{ii}(B)	0.903	2.146	3.034	167.5	b	$R_4^4(24)$	D(type 2)			
c	Nb2−Hb2B(B)···Na3 ^{iii}(A)	0.967	2.478	3.422	165.4	c	C(18)	$R_4^4(44)$	D(type 3)		
d	Na1−Ha1(A)···Nb3^{iv}(B)	0.889	2.271	3.049	146.0	d	$R_4^4(24)$	C(18)	$R_4^4(44)$	D(type 4)	
e	Nb2−Hb2A(B)···Ob2^{v}(B)	0.815	2.754	3.359	132.6	e	C(8);D	C(8);D	C(8);D	C(8);D	C(8)(type 1)	
f	Na2−Ha2A(A)···Oa2^{vi}(A)	0.828	2.377	3.058	140.1	f	C(8);D	C(8);D	C(8);D	C(8);D	C(8);C(8)	C(8)(type 1)

XIV	D−H(X)···A(Y)[e]	D−H	H···A	D···A	D−H···A	a
a	N1−H1(A)···O2^{i}(A)	0.952	1.913	2.862	174.25	a	C(4)(type 1)

[a] D−H(X)···A(Y), where X and Y corresponds to molecule A or B of the asymmetric unit. [b] Symmetry code: (i) $x, y-1, z$. [c] Symmetry code: (i) $-x+1/2, -y+1, z-1/2$; (ii) $x+1, y, z$; (iii) x, y, z; (iv) $x, -y+1/2, z-1/2$. [d] Symmetry code: (i) $x+1, -y+1, z+1/2$; (ii) $-x+1\ 1/2, -y+1\ 1/2, -z+2$; (iii) $x+1, y+1, z+1$; (iv) $-x+1, y+1, -z+1\ 1/2$; (v) $x+1, y+1, z+1$; (vi) $x+1, y+1, z+2$. [e] Symmetry code: (i) x, y, z.

dx.doi.org/10.1021/cg1012389 |*Cryst. Growth Des.* 2011, 11, 1067–1081

Table 4. Graph Set Notations of the Hydrogen Bond Networks of the Crystal Structures Studied

First level graph sets	
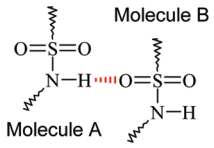 *D*(type 1): **XIII** (AB^a)	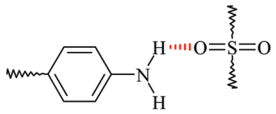 *D*(type 2): **IV**(AB^a; BA^a), **V**(AB^a; BA^a), **VI**(AB^a), **XIII** (AB^a)
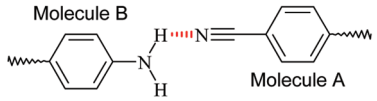 *D* (type 3): **XIII** (AB^a)	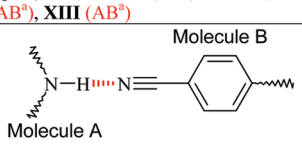 *D* (type 4): **XIII** (AB^a)
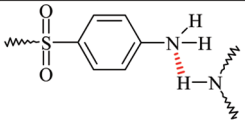 *D* (type 5): **V** (AB^a; BA^a)	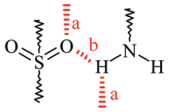 *C*(2): **XII**
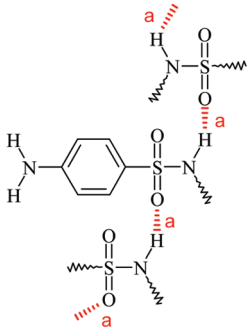 *C*(4) (type 1): **I**, **II**, **III**, **VIII**, **IX**, **XIV**	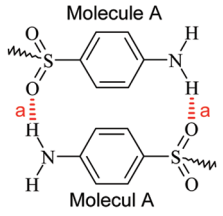 $R_2^2(16)$: **V**(AA^a)
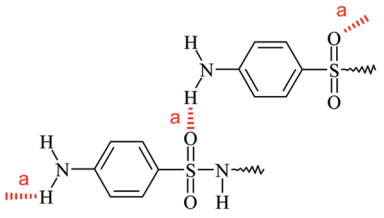 *C*(8) (type 1): **IV**, **VI**, **VII**, **VIII**, **IX**, **X**, **XII**	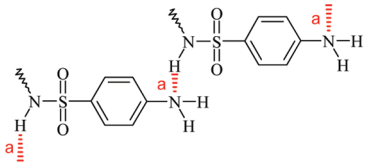 *C*(8) (type 2): **IV**, **VI**, **VII**, **X**, **XII**
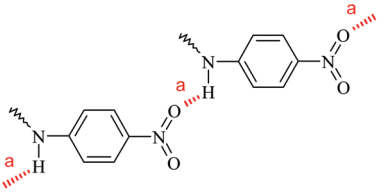 *C*(8) (type 3): **XI**	
Second level graph sets	
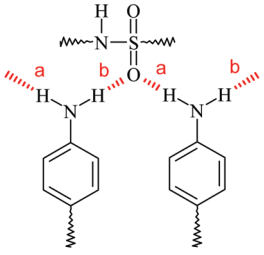 $C_2^1(4)$ (type 2): **VIII**, **IX**,	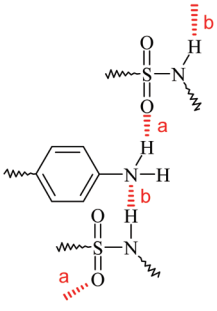 $C_2^2(6)$(type 1): **IV**(AA^a, BB^a) , **V**(AB^a,BA^a), **VI** (AA^a, BB^a), **VII**, **X**, **XII**

dx.doi.org/10.1021/cg1012389 |*Cryst. Growth Des.* 2011, 11, 1067–1081

Table 4. Continued

Second level graph sets	
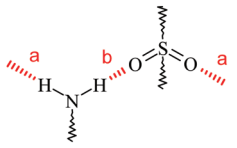 $C_2^2(6)$ (type 2): **IV**(AA^a, BB^a), **V**(AB^a, BA^a), **VII**, **VIII**, **IX**, **X**, **XII**	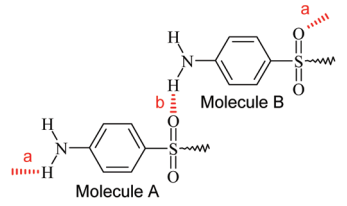 $C(16)$ (type 1): **IV**(AB^a), **V**(AB^a)
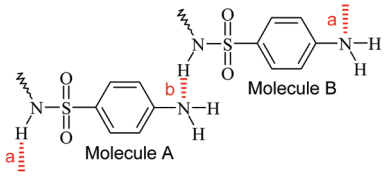 $C(16)$ (type 2): **V**	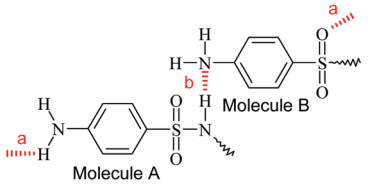 $C(16)$ (type 3): **V**
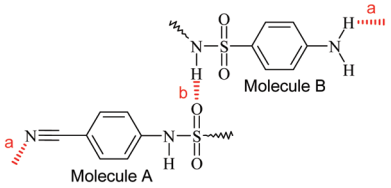 $C(18)$ (type 1): **XIII**	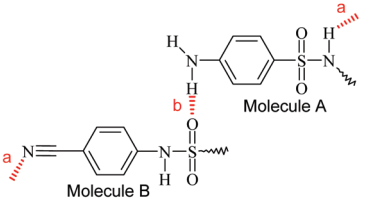 $C(18)$ (type 2): **XIII**
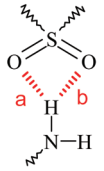 $R_1^2(4)$ (type 1): **VIII**, **IX**	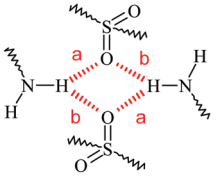 $R_2^2(4)$ (type 2): **VIII**, **IX**
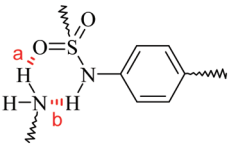 $R_2^2(6)$: **IV**(AA^a,BB^a), **V**(AB^a), **VII**, **X**, **XII**	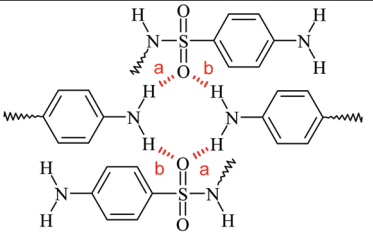 $R_4^2(8)$: **VIII**, **IX**
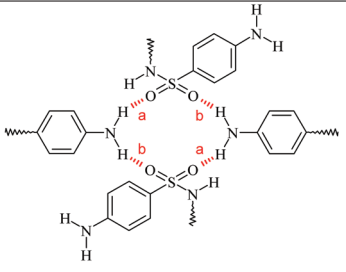 $R_4^4(12)$: **VIII**, **IX**	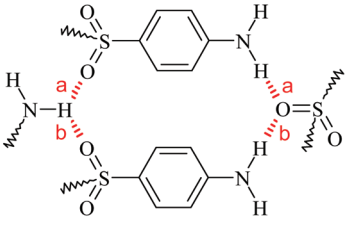 $R_3^3(18)$: **XII**

(6) > C(8)-3 = D-1 = D-3 = D-4 = $R_2^2(16)$ (1 time). The presented discrimination is quite conditional because for the chosen compound the graph set assignment can occur several times with different hydrogen bonds. Usually this fact is connected with increase of a number of molecules in asymmetric unit of crystal lattice. By our opinion, increase of a number of the same type of graph set assignment within the substance leads to a decrease of the accuracy of experimental measurements (saturation vapor pressure, melting point, fusion enthalpy, and so on).

It is interesting to analyze if there is some regularity between E^{HB} (within the same topological graph) and the molecular van der Waals volume. It should be noted that the graph set notation C(8)-1 is observed for many compounds. Moreover, for each substance this graph can appear several times since it can be created by different hydrogen bonds. The analogous picture is

dx.doi.org/10.1021/cg1012389 |*Cryst. Growth Des.* 2011, 11, 1067–1081

Table 5. First Level Graph Set Notations of the Hydrogen Bonds Networks of Sulfonamides Studied, Frequency of Appearance, and Energies (E^{HB}, kJ·mol^{-1}) of the Hydrogen Bonds

Notations	Type			E^{HB}, kJ·mol^{-1}					
				1	2	3	4	5	6
C(8)	1	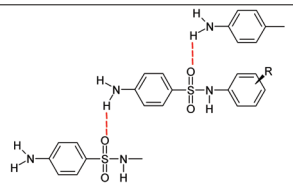	**IV**	8.0	7.1	1.5	0.3		
			VI	8.1	5.3	2.6			
			VII	10.6	5.4				
			VIII	4.7	4.5	3.4	1.4		
			IX	5.6	5.4	3.9	1.0		
			X	6.0	3.2				
			XII[a]	5.6(a)	1.0(c)	0.2(b)			
			XIII[a]	4.6(f)	1.5(e)				
C(8)	2	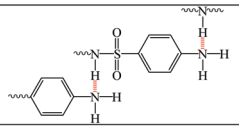	**IV**	12.1	11.8				
			VI	8.6	8.2				
			VII	8.6					
			X	2.1					
			XII[a]	7.5(d)					
C(8)	3	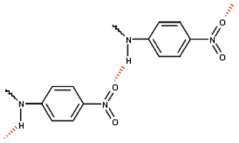	**XI**[a]	14.7(a)					
C(4)	1	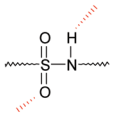	**I**	13.6					
			II	12.3					
			III	14.9					
			VIII	7.4					
			IX	9.4					
			XIV[a]	18.1(a)					
D	1	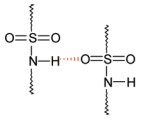	**XIII**[a]	11.2(a)					
D	2	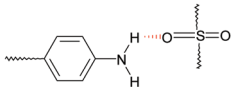	**IV**	1.0	0.3				
			V	2.3	11.0	7.2	2.3	10.0	11.0
			VI	0.5					
			XIII[a]	12.8(b)					
D	3	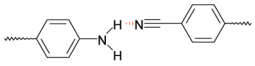	**XIII**[a]	5.4(c)					
D	4	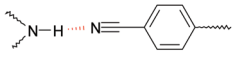	**XIII**[a]	6.4(d)					
$R_2^2(16)$	1	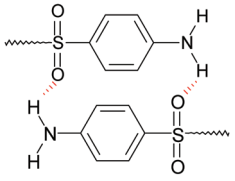	**V**	2.7					

[a] Labeling corresponds to the hydrogen bonds of Table 3.

observed for C(8)-2, whereas C(4)-1 motif is the only one for all the substances where this graph appears (in other words, when C(4) appears, there are no other hydrogen bonds in the structure). The hydrogen bond energies versus molecular van der Waals volumes for C(4)-1 (a), C(8)-2 (b), and C(8)-1 (c) motives are summarized in Figure 5. For C(4)-1 a correlation between the noted variables is observed: with an increase of the molecular van der Waals volume the E^{HB}-value decreases. For C(8)-2 this trend is not obvious, whereas for C(8)-1 the correlation is not observed at all. This behavior can be explained by the following reasons. For the compounds, where the regularity is observed (C(4)-1 graphs), there is only one hydrogen bond per molecule (no alternative hydrogen bonds). Therefore, a variation of the molecular van der Waals volume does not lead to a change of the molecular packing in the crystal lattice (because it remains the same type of graph set) and affects only the change of geometry and strength of the hydrogen bonds. On the other hand, for the compounds with C(8)-1 and C(8)-2 motifs, besides these notations, there are alternative ones. As a result, the increase of molecular van der Waals volume is relaxed by all the hydrogen bonds available.

Packing Architecture Analysis. The molecular packing architecture of crystals depends on the molecular structure and topology. The compounds under consideration are structurally similar. Therefore, variations of size, nature, and position of substituents make it possible to analyze the influence of these factors on the packing architecture. It is interesting to note that the free volumes per molecule in the crystal lattices range within the limits 103−107 Å^3 and are practically independent from the molecular van der Waals volume (Figure 6) (except **I**, **VI**, **XI**, and

dx.doi.org/10.1021/cg1012389 |*Cryst. Growth Des.* 2011, 11, 1067–1081

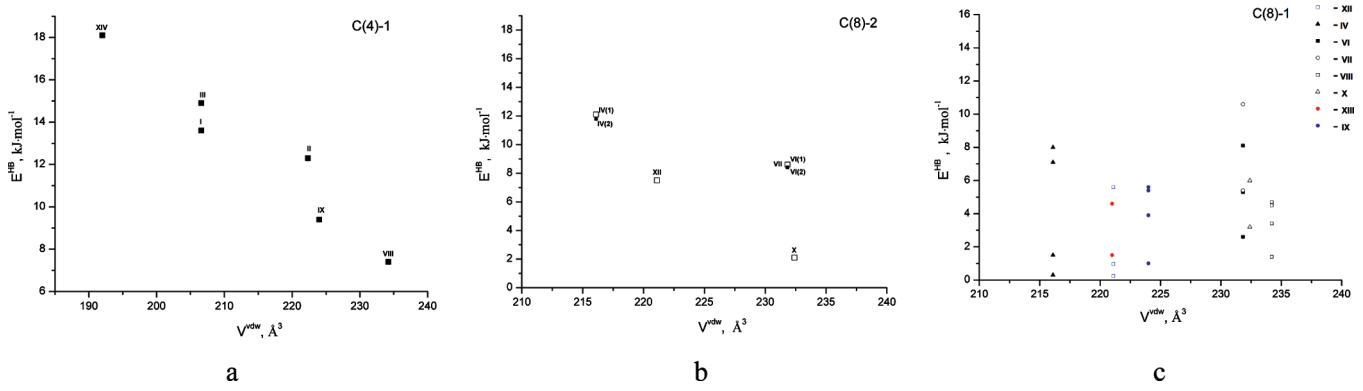

Figure 5. Plot of the hydrogen bond energies versus the molecular van der Waals volumes of studied substances for C(4)-1 (a), C(8)-2 (b), and C(8)-1 (c) motives.

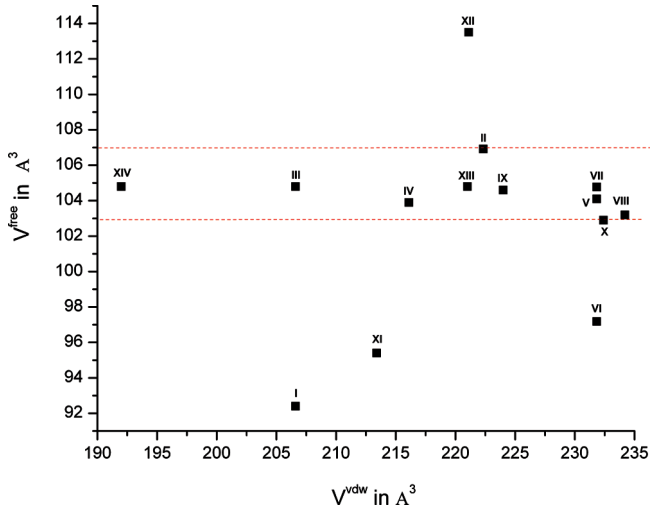

Figure 6. Relationship between the free molecular volumes (V^{free}) in the crystal lattices and the van der Waals volumes (V^{vdw}) of the compounds.

XII). The deviation of the discussed values for **VI** is probably connected with the following fact. The crystal lattices of **IV** and **VI** are isomorphic:[11] the same space groups - orthorhombic $Pna2_1$; V_{cell}(**IV**) = 2560.0(9) and V_{cell}(**VI**) = 2632.1(9) Å^3; V^{vdw}(**IV**) = 216.1 and V^{vdw}(**VI**) = 231.8 Å^3; V^{free}(**IV**) = 103.9 and V^{free}(**VI**) = 97.2 Å^3. Therefore, the accommodation of the additional Cl-atom of compound **VI** (in comparison with **IV**) occurs in the free volume of the unit cell of substance **IV**. Compounds **I**, **XI**, and **XII** require a more detailed analysis. It can be assumed that the substances, included in the window, have identical molecular packing architecture, whereas **I**, **XI**, and **XII** sulfonamides have essential elements of distinction.

In order to understand the influence of various molecular fragments on crystal lattice energy, we used the approach applied by us earlier.[25] The molecule was conditionally divided into a certain number of fragments, depending on the molecular topology. Segmentation for the six fragments (as a common case) is shown in Scheme 2. After that we calculated the contribution of nonbonded van der Waals interactions to the packing energy from different fragment pairs of adjacent molecules. The results of the calculation for various energetic terms of the SA crystal lattices are shown in Figure 7.

Let us first consider the SAs with two substituents at the second phenyl ring (**V**, **VI**, **VII**, **X**) (Figure 8). The main contributions,

Scheme 2

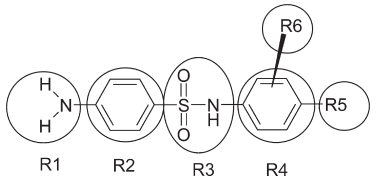

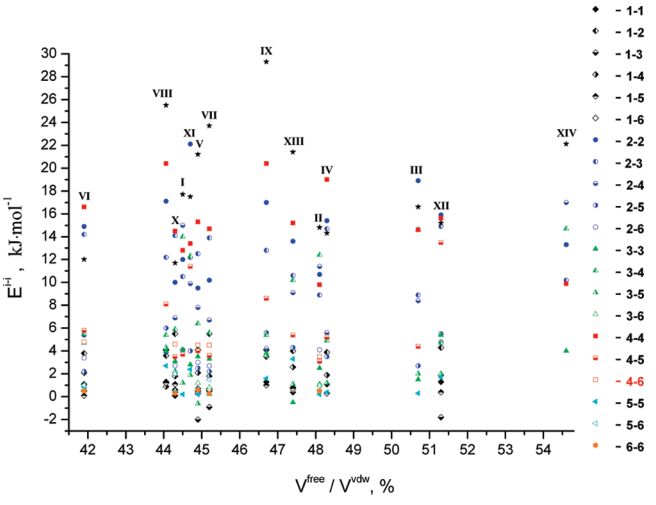

Figure 7. Plot of the contributions of nonbonded van der Waals interactions to the packing energy from different fragment pairs of adjacent molecules (E^{i-i}) versus V^{free}/V^{vdw} for studied compounds (asterisks correspond to correction for the hydrogen bond energy).

stabilizing the crystal lattices, correspond to interactions between R_4-R_4; R_2-R_3 and R_2-R_2. Moreover, when one of the substituents is situated at para- position of Ph2, an inversion of R_2-R_3 and R_2-R_2 contributions to the crystal lattice stabilization is observed: for **VI** - $E(R_4-R_4) > E(R_2-R_2) > E(R_2-R_3)$, whereas for **V**, **VII**, **X** - $E(R_4-R_4) > E(R_2-R_3) > E(R_2-R_2)$. The absolute values of the maximal (R_4-R_4) contributions are approximately the same (within 1 kJ·mol^{-1}). The analogous conclusion can be made for R_2-R_3 as well. The R_2-R_2 contributions (interactions between the second phenyl rings of adjacent molecules in the crystal lattices) for compounds **V**, **VII**, **X** do not differ essentially from each other; however, they are 5 kJ·mol^{-1}

dx.doi.org/10.1021/cg1012389 |*Cryst. Growth Des.* 2011, 11, 1067–1081

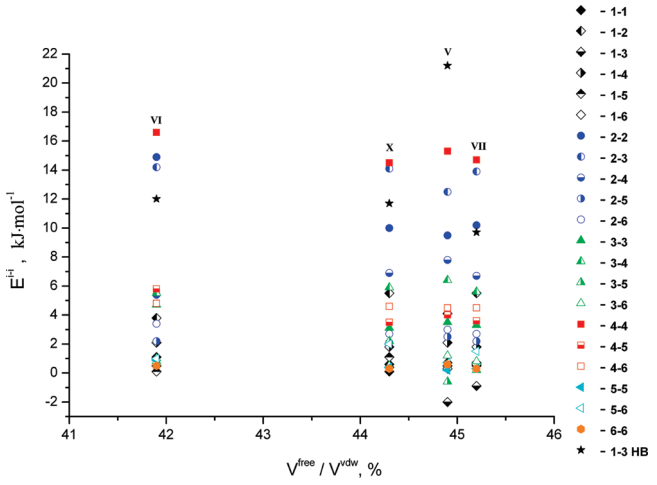

Figure 8. Plot of E^{i-i} versus V^{free}/V^{vdw} for **V**, **VI**, **VII**, and **X**.

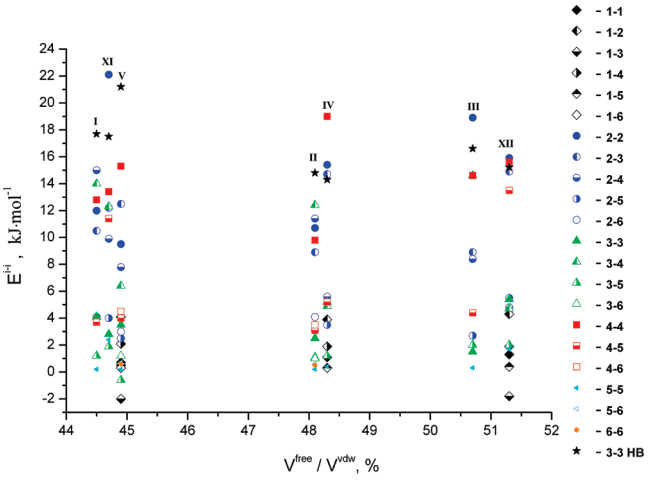

Figure 9. Plot of E^{i-i} versus V^{free}/V^{vdw} for **I**−**V**, **VII**, and **XI**.

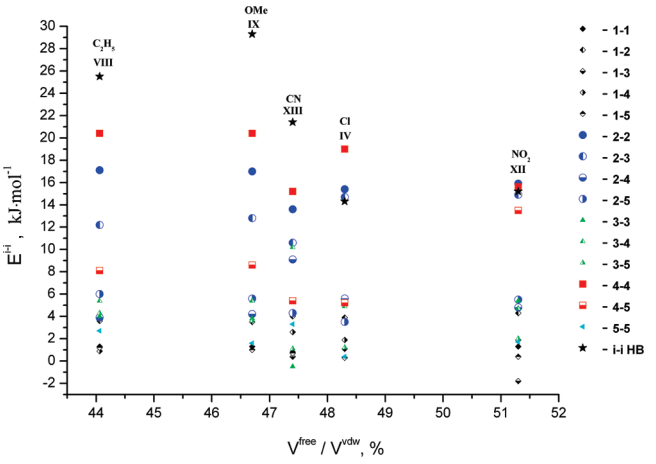

Figure 10. Plot of E^{i-i} versus V^{free}/V^{vdw} for **IV**, **VIII**, **IX**, **XII**, and **XIII**.

lower than the analogous value for **VI**. Thus, for the sulfonamides with substituents at the para position of Ph2 the main stabilizing crystal lattice contributions correspond to the interactions between the identical phenyl fragments (R_4-R_4 and R_2-R_2) of adjacent molecules. For the rest of the compounds the bridge connecting the two phenyl rings intervenes in the energetic apportionment: R_4-R_4 and R_2-R_3. It should be noted that for **VI** contributions of R_2-R_4 (Ph1-Ph2) and R_4-R_5 (Ph2-R_5) interactions are equal, whereas for the rest of the substances $R_2-R_4 > R_4-R_5$ by 4 kJ·mol^{-1}. For SA **VI** there is a big energetic slit (8 kJ·mol^{-1}) between the strongest contributions (R_4-R_4; R_2-R_3 and R_2-R_2) and the other ones. For the other SAs, this slit is not observed due to infilling them with R_2-R_2; R_2-R_3 and R_2-R_4 interactions. One more peculiarity of the fragmental interactions consists of the following: for **VI** - $E(R_4-R_5) > E(R_1-R_2)$, whereas for **V**, **VII**, **X** the opposite regularity is observed.

The fragments of the molecules take part in creating hydrogen bonds. Therefore, in order to be correct, we tried to introduce a correction on the hydrogen bonding energy at the R_1-R_3 interaction (Figure 8 asterisks): for **VI** - $E^{tot}(R_1-R_3)$ = 12 kJ·mol^{-1}; for **V** - $E^{tot}(R_1-R_3)$ = 21.2 kJ·mol^{-1}; for **VII** - $E^{tot}(R_1-R_3)$ = 9.7 kJ·mol^{-1}; for **X** - $E^{tot}(R_1-R_3)$ = 11.7 kJ·mol^{-1}. It is not difficult to see that the terms from interactions with account of the hydrogen bond contribute an essential correction to the packing energy. For example, this term for substance **V** exceeds the maximal term $E(R_4-R_4)$ by 5 kJ·mol^{-1} and is dominant, whereas for **X** this contribution is third and for **VI** and **VII** fourth. It is interesting to note that contributions of R_1-R_3 interactions (with account of hydrogen bond), creating graph sets C(8) (**VI**, **VII**, **X**), have approximately the same values (10−12 kJ·mol^{-1}). In its turn the analogous contribution for **V** exceeds the previous ones considerably. Moreover, the hydrogen bonds are integrated in D organization of hydrogen bond networks. So, asymmetric molecular structure (**V**) leads to D organization of hydrogen bond networks and a considerable contribution of the hydrogen bonding energy to the packing energy. This behavior is not observed for more symmetric molecules.

Let us consider the packing energy of the molecules, where the first fragment does not contain NH_2-group: **I**, **II**, **III**, **XI** (Figure 9). It should be mentioned that for the para- substituted molecules (**III** and **XI**) the apportionment of the fragmental contributions differs essentially from the other substituted molecules (**I** and **II**). For example, the dominant contribution for the para-substituted SA corresponds to the interactions between the second fragments of the molecules $E(R_2-R_2)$ (Ph1−Ph1 interactions), whereas for the rest of the compounds the main contributions to packing energy correspond to the two practically equal terms: $E(R_2-R_4)$ (Ph1−Ph2) and $E(R_3-R_4)$ (bridge-Ph2). Moreover, the main contributions to the packing energy for the para- substituted SA exceed substantially the analogous term for the other compounds. The impact of the substituent nature at the para position can be analyzed on compounds **III** and **XI**. The crystal **XI** has a denser molecular packing in comparison with **III**: β(**XI**) = V^{free}/V^{vdw} = 44.7 < β(**III**) = 50.7%. Probably this fact determines (at approximately the same terms $E(R_2-R_4)$ and $E(R_4-R_4)$) the prevalence of the terms $E(R_2-R_2)$ and $E(R_4-R_5)$ for **XI** (NO_2-) in comparison with **III** (Cl-). If we compare SA **I** and **II** (i.e., the molecules differing by additional Cl- atom at meta- position of the second phenyl ring), the dominant energy contributions are the same ($E(R_3-R_4)$, $E(R_2-R_4)$, $E(R_2-R_2)$, and $E(R_2-R_3)$), but their consecution is slightly changed.

As we had done before, we tried to introduce a correction for hydrogen bonding energy in the packing energy of compounds **I**, **II**, **III**, **XI**. In contrast to the previous SAs (with NH_2- groups at Ph1), this group of the compounds creates hydrogen bonds between R_3-R_3 fragments, forming C(4) hydrogen bond networks. The result of the corrections is presented in Figure 9 by

dx.doi.org/10.1021/cg1012389 |*Cryst. Growth Des.* 2011, 11, 1067–1081

Table 6. Temperature Dependencies of Saturation Vapor Pressure of the Compounds Studied

XI[a]		XII[b]		XIII[c]		XIV[d]	
t [°C]	P [Pa]	t [°C]	P [Pa]	t [°C]	P [Pa]	t [°C]	P [Pa]
107.0	9.47×10^{-3}	132.4	1.50×10^{-3}	147.0	6.74×10^{-3}	75.9	2.78×10^{-2}
111.0	1.55×10^{-2}	136.3	2.18×10^{-3}	147.8	7.23×10^{-3}	78.3	3.48×10^{-2}
112.0	1.72×10^{-2}	139.7	2.30×10^{-3}	148.2	7.91×10^{-3}	80.4	4.22×10^{-2}
114.0	2.09×10^{-2}	142.0	3.41×10^{-3}	151.6	1.13×10^{-2}	81.6	4.74×10^{-2}
117.0	2.84×10^{-2}	144.1	4.01×10^{-3}	153.4	1.36×10^{-2}	83.0	5.61×10^{-2}
118.0	3.17×10^{-2}	145.6	4.34×10^{-3}	155.2	1.66×10^{-2}	84.3	6.56×10^{-2}
119.0	3.47×10^{-2}	146.9	5.46×10^{-3}	156.5	1.94×10^{-2}	85.5	7.20×10^{-2}
120.0	3.88×10^{-2}	148.4	5.63×10^{-3}	158.2	2.11×10^{-2}	86.3	7.81×10^{-2}
121.0	4.04×10^{-2}	150.1	6.16×10^{-3}	158.6	2.28×10^{-2}	87.8	9.44×10^{-2}
122.0	4.64×10^{-2}	151.5	7.30×10^{-3}	159.2	2.33×10^{-2}	89.6	10.9×10^{-2}
123.5	5.13×10^{-2}	153.1	8.92×10^{-3}	159.9	2.63×10^{-2}	91.1	12.5×10^{-2}
128.0	8.37×10^{-2}	155.6	1.05×10^{-2}	161.6	3.17×10^{-2}	92.1	13.7×10^{-2}
128.5	8.63×10^{-2}	158.2	1.28×10^{-2}	162.6	3.58×10^{-2}	93.3	16.1×10^{-2}
		158.9	1.41×10^{-2}	164.0	4.24×10^{-2}	94.4	18.1×10^{-2}
		162.0	1.81×10^{-2}	164.4	4.37×10^{-2}	96.2	21.5×10^{-2}
		165.1	2.28×10^{-2}				

[a] $\ln(P[\text{Pa}]) = (35.8 \pm 0.5) - (15378 \pm 187)/T$; $\sigma = 2.7 \times 10^{-2}$; $r = 0.999$; $F = 6742$; $n = 13$. [b] $\ln(P[\text{Pa}]) = (30.5 \pm 0.8) - (15041 \pm 317)/T$; $\sigma = 6.4 \times 10^{-2}$; $r = 0.9964$; $F = 2247$; $n = 16$. [c] $\ln(\text{P[Pa]}) = (41.3 \pm 0.6) - (19459 \pm 272)/T$; $\sigma = 3.2 \times 10^{-2}$; $r = 0.9996$; $F = 5129$; $n = 15$. [d] $\ln(\text{P[Pa]}) = (33.9 \pm 0.4) - (13092 \pm 131)/T$; $\sigma = 2.3 \times 10^{-2}$; $r = 0.9988$; $F = 9916$; $n = 15$.

asterisks. It is not difficult to see that the values of the contributions are approximately situated within 3 kJ·mol^{-1}. The contributions for substances **I** and **II** are dominant, whereas for **III** and **IX** second throughout the energy. Thus, it can be assumed that hydrogen bond networks of SA with substituents at the para position will have less impact on the physicochemical properties in comparison with the substituents at other positions. It can be assumed that the first step of the nucleation process of the considered compounds starts from creating hydrogen bonds (self-assembly), whereas the second step can be connected with growing the nucleus by the most dominant fragments interactions. In the case of SAs **III** and **XI** the growth is driven by R_2-R_2 interactions (Ph1—Ph1). The situation with compounds **I** and **II** is different from the previous one. As dominant contributions (if it does not take into account hydrogen bonding) several fragmental interactions can appear: $E(R_3-R_4)$, $E(R_2-R_4)$, $E(R_2-R_2)$, and $E(R_2-R_3)$. This variability can bring disordering of the molecules in the crystals or creating various types of defects during the growing process. On the contrary, for compounds **III** and **XI** more perfect single crystals can be expected.

Let us consider the identical molecules with and without NH_2-groups at the first phenyl ring: **II** and **V**, **III** and **IV**, **XI** and **XII**. It is interesting to note,= that introducing the NH_2- group in compounds **II** and **III** (it gives **V** and **IV**) leads to an increase of molecular packing density in the crystals: $\beta(\mathbf{V}) = V^{\text{free}}/V^{\text{vdw}} = 48.1 < \beta(\mathbf{II}) = 44.9\%$; $\beta(\mathbf{IV}) = 48.3 < \beta(\mathbf{III}) = 50.7\%$. In contrast to this, for substances **XI** and **XII** the opposite regularity is observed: $\beta(\mathbf{XI}) = 44.7 < \beta(\mathbf{XII}) = 51.3\%$. For the compounds with the asymmetric location of Cl- atoms (**II** and **V**) the fragments, taking part in creating hydrogen bonds, bring in the dominant contribution in the crystal packing energy. For the SAs with the location of Cl- atom at para- position (**III** and **IV**) the noted terms are not dominant. It is evident, that with introducing the NH_2-group an essential redistribution of the terms in the crystal packing energy is observed. For example, the four maximal contributions of SA **II** can be arranged as: $E(R_3-R_4) > E(R_2-R_4) > E(R_2-R_2) > E(R_4-R_4)$, whereas for SA **V**: $E(R_4-R_4) > E(R_2-R_3) > E(R_2-R_2) > E(R_2-R_4)$. Moreover, the strongest terms of compound **II** are separated from the weakest ones by a 5 kJ·mol^{-1} "energetic slit". For SA **V** the mentioned slit is not observed. Similarly, the terms for SA **III** can be arranged as: $E(R_2-R_2) > E(R_4-R_4) = E(R_3-R_4)$, whereas for SA **IV**: $E(R_4-R_4) > E(R_2-R_2) > E(R_2-R_3)$. The "energetic slit" for SA **IV** is equal to 9 kJ·mol^{-1}, whereas for SA **III** — to 6 kJ·mol^{-1}.

Finally, let us consider the contributions in the packing energy made by different fragments of para-substituted SA **IV** (Cl-), **VIII** (C_2H_5-), **IX** (OMe-), **XII** (NO_2-), **XIII** (CN-) (Figure 10). For the studied compounds, the strongest contributions in the packing energy cab be arranged as $E(R_4-R_4) > E(R_2-R_2) > E(R_2-R_3)$. For the crystals with big values of molecular packing density, a considerable dispersion of the energetic terms is observed. However, with a decrease of the molecular packing density the differences between the contributions become negligible.

If we take into account the contributions to the packing energy from the fragments creating hydrogen bonds, the following situation is observed (Figure 10). The discussed terms exceed the other ones until reaching the defined value of the molecular packing density. After passing the point, the difference between the contributions becomes negligible. For all SAs the para-substituent interacts more strongly with the second phenyl ring in comparison to the first one: $E(R_4-R_5) > E(R_2-R_5)$. Moreover, this tendency is quite evident for **XII** (NO_2-).

Sublimation Characteristics. The temperature dependencies of saturated vapor pressure of **V**—**VII** are shown in Table 6. The thermodynamic functions of the drugs sublimation, fusion, and vaporization processes are presented in Table 7.

We have tried to search the correlation between the sublimation thermodynamic functions and the descriptor describing the sum of H-bond acceptor factors (ΣC_a) of the molecule, as it was done before to analyze the conformational states of SAs. The dependence between the sublimation Gibbs energies and ΣC_a is shown in Figure 11. It is not difficult to see that with an increase

Table 7. Thermodynamic Characteristics of Processes of Sublimation, Fusion, and Vaporization of the Compounds Studied

	XI	XII	XIII	XIV
ΔG^{298}_{sub} [kJ·mol^{-1}]	67.7	78.0	88.0	53.4
ΔH^{T}_{sub} [kJ·mol^{-1}]	127.9 ± 1.6	125.1 ± 2.6	161.8 ± 2.3	108.9 ± 1.1
ΔH^{298}_{sub} [kJ·mol^{-1}]	132.5 ± 1.6	131.4 ± 2.6	168.3 ± 2.3	111.5 ± 1.1
$C^{298}_{p,cr}$ [J·mol^{-1}·K^{-1}]^a	327.5	340.1	326.3	280.4
$T\cdot\Delta S^{298}_{sub}$ [kJ·mol^{-1}]	64.7	53.4	80.3	58.1
ΔS^{298}_{sub} [J·mol^{-1}·K^{-1}]	217 ± 7	179 ± 7	269 ± 9	195 ± 6
ς_H [%]^b	67.2	71.1	67.7	65.7
ς_{TS} [%]^b	32.8	28.9	32.3	34.3
T_m [K]	411.3 ± 0.2	438.9 ± 0.2	451.5 ± 0.2	383.5 ± 0.2
ΔH^{T}_{fus} [kJ·mol^{-1}]	28.7 ± 0.5	27.9 ± 0.5	30.9 ± 0.5	23.5 ± 0.5
ΔH^{298}_{fus} [kJ·mol^{-1}]	20.8	18.9	20.4	18.3
ΔS^{T}_{fus} [J·mol^{-1}·K^{-1}]^c	69.8	63.6	68.4	61.3
ΔH^{298}_{vap} [kJ·mol^{-1}]	111.7	112.5	147.9	93.2

^{a} $C^{298}_{p,cr}$ has been calculated by additive scheme with the following group values (in J·K^{-1}·mol^{-1}): C_p(−SO_2-) = 88.7; C_p(quaternary aromatic C sp^2 = C_aR-) = 8.5; C_p(tertiary aromatic C sp^3 = C_aH-) = 17.5; C_p(−NH-) = −0.3; C_p(-NO_2) = 56.1; C_p(−NH_2) = 21.6; C_p(−CN) = 42.3 the error of the calculation procedure corresponds to significant digit; ^{b} $\varsigma_H = (\Delta H^{298}_{sub}/(\Delta H^{298}_{sub} + T\Delta S^{298}_{sub}))\cdot 100\%$; $\varsigma_{TS} = (T\Delta S^{298}_{sub}/(\Delta H^{298}_{sub} + T\Delta S^{298}_{sub}))\cdot 100\%$. ^{c} $\Delta S_{fus} = \Delta H_{fus}/T_m$.

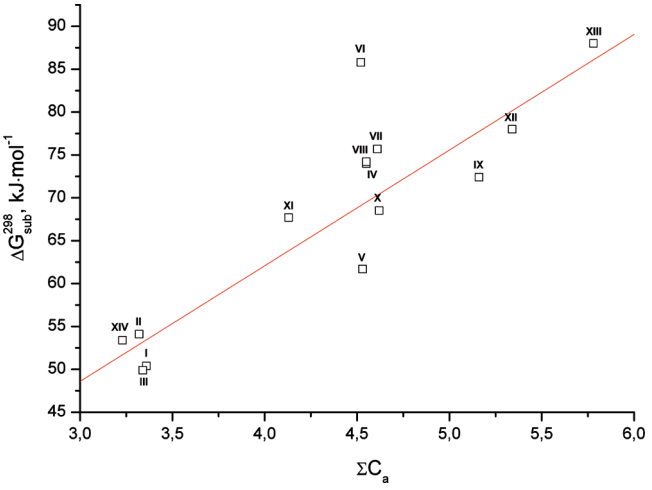

Figure 11. Relationship between the sublimation Gibbs energies (ΔG^{298}_{sub}) and the sum of H-bond acceptor factors (ΣC_a).

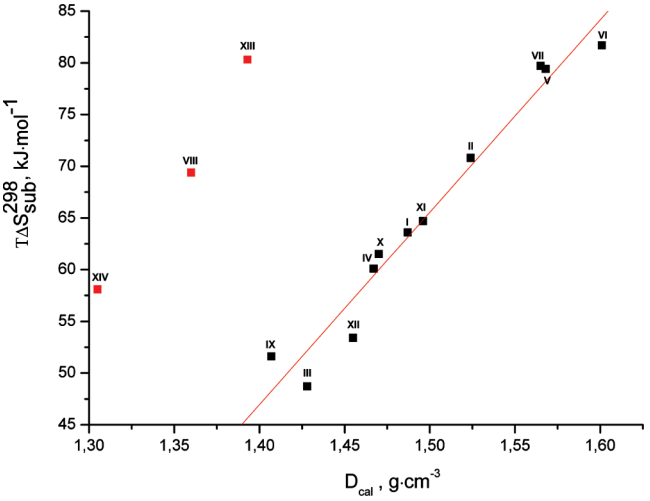

Figure 12. Correlation between the sublimation entropic terms ($T\Delta S^{298}_{sub}$) and calculated molecular densities (D_{cal}) in the crystal lattices (see text for numbering of the compounds).

of the molecule acceptor ability to create hydrogen bonds the sublimation Gibbs energy increases as well. Unfortunately, substance **VI** deviates from the trend. If we do not take this value into consideration, the discussed trend can be described by the regression equation:

$$\Delta G^{298}_{sub} = (8 \pm 6) + (13.5 \pm 1.5)\Sigma C_a$$
$$r = 0.9375; \sigma = 4.3; n = 13 \qquad (9)$$

Thus, the Gibbs energy of the compound belonging to the group under consideration can be estimated simply on the basis of the structural formula. It should be noted that the mentioned thermodynamic function is very important for predicting the solubility values of poorly soluble drugs, since the calculation approaches to estimating solvation/hydration terms have been recently improved greatly.

As the D_{cal} parameter is an entropic characteristic of a crystal, we tried to compare these values with the entropic terms of the sublimation process ($T\Delta S^{298}_{sub}$) of the compounds (Figure 12). It is not difficult to see that all data break up into two branches. Moreover, it is difficult to explain why the compounds **VIII**, **XIII**, and **XIV** create their own branches. The rest of the SAs can be described by the correlation equation:

$$T\Delta S^{298}_{sub} = (-214 \pm 19) + (186 \pm 13)D_{cal}$$
$$r = 0.980; \sigma = 2.44; n = 11 \qquad (10)$$

The experimentally obtained crystal density values can be expected to be correlated with the calculated ones. Therefore, the entropic sublimation term can be directly estimated by the experimental density values, without any knowledge of the crystal structure. If we take into account the eqs 8 and 9 obtained before, the sublimation enthalpy term can be estimated. In other words, on the basis of crystal density values and structural formulas it is possible to describe the sublimation thermodynamic functions of the processes for the studied group of molecular crystals.

It is well-known that the melting point (T_m) and fusion enthalpy (ΔH^{T}_{fus}) of molecular crystals are usually used in pharmaceutics

dx.doi.org/10.1021/cg1012389 |Cryst. Growth Des. 2011, 11, 1067–1081

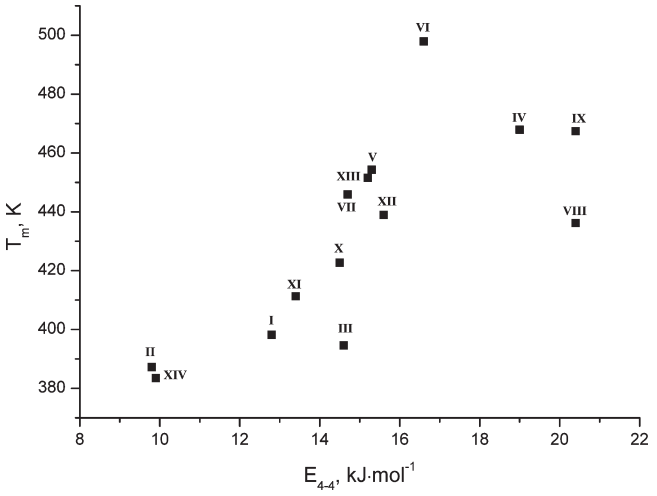

Figure 13. Relationship between the melting points and E^{4-4} contributions in the packing energy made by the nonbounded van der Waals interactions.

as parameters modeling crystal lattice energy. As an example we can present the general solubility equation obtained by Yalkowsky and Valvani.[26] The popularity of the parameters is connected with the fact that they can be obtained in a very easy way through the routine DSC method. The melting points and fusion enthalpies of the studied SAs are presented in Table 7. It should be mentioned that in the literature there are still certain discussions about the nature and mechanism, determining the outlined parameters.[27] We tried to find out the correlation between the melting points and the contributions in the packing energy made by the nonbounded van der Waals interactions. It is interesting to note that a linear trend is observed between T_m and E_{4-4}: the melting point values are raised while the interactions between the second phenyl fragments are increased as well (Figure 13). As it was shown before (Figure 7), E_{4-4} term in the packing energy is dominant in comparison with the other ones. Therefore, it can be assumed that the melting process starts with the loss of contact between the second phenyl fragments of SA. The hydrogen bonding energy between definite fragments of adjacent molecules can be higher or lower than E_{4-4} (it depends on the compounds). Therefore, it could be assumed that in the case when $E^{HB} < E_{4-4}$ the hydrogen bonds break up before the melting temperature. In the opposite case, breaking up of the hydrogen bonds goes on at higher temperatures in comparison with the melting one.

CONCLUSION

The crystal structures of four sulfonamides (**XI**−**XIV**) have been solved by X-ray diffraction experiments. Comparative analysis of molecular conformational states has been carried out. All the considered compounds break up into two conformational populations (if the angles between the phenyl rings are taken into account). The first one includes SAs with angles 47° < ∠Ph1−Ph2 < 67°, whereas the second one, SAs with angles: 77° < ∠Ph1−Ph2 < 92°. For the low-angle conformational population, the angle between the phenyl rings increases with decreasing the bridge integral mobility. For the large-angle populations, a dependence with the extreme value for the compound **XIIIB** is observed. On the basis of the correlation analysis, we found out that donor−acceptor interactions and hydrogen bonding in the crystals lead to a reduction of the bridge mobility.

Hydrogen bond network topology of the sulfonamides by the graph set notations has been analyzed. The graph set notations can be arranged (according to the frequency of their appearance in the studied crystals) in the following way: C(8)-1 (type 1) > C(4)-1 > C(8)-2 > D-2 > C(8)-3 = D-1 = D-3 = D-4 = $R_2^2(16)$. We have also studied the relationships between hydrogen bond energies and molecular van der Waals volumes within the definite graph set assignments. For C(4)-1 a correlation between the noted variables is observed: with an increase of the molecular van der Waals volume the E^{HB}-value decreases. For C(8)-2 this trend is not obvious, whereas for C(8)-1 the correlation is not observed at all.

The free volumes per molecule in the crystal lattices of SAs range within the limits of 103−107 Å^3 and are practically independent from the molecular van der Waals volume. The influence of various molecular fragments on the crystal packing energy was analyzed. For most of the studied compounds the main contributions, stabilizing the crystal lattices, correspond to the interactions between: the second phenyl rings Ph2−Ph2; the first ones Ph1−Ph1 and the bridge − Ph1. We have also found the correlation between the melting points and the contributions in the packing energy from the nonbounded van der Waals interactions: the melting point values rise, while the interactions between the second phenyl fragments increase as well.

The thermodynamic aspects of the sulfonamide sublimation processes have been studied by investigating the temperature dependence of vapor pressure by means of transpiration method. A correlation between the Gibbs energy of sublimation and the molecular H-bond acceptor factors was found. Also a regression equation was derived describing the correlation between the sublimation entropy terms and the crystal density data calculated by the X-ray diffraction results. These dependencies allow us to predict the sublimation thermodynamic parameters not knowing more than the molecular formula and crystal density.

ASSOCIATED CONTENT

Supporting Information. The cif files of the **XI**−**XIV** compounds. This material is available free of charge via the Internet at http://pubs.acs.org.

AUTHOR INFORMATION

Corresponding Author

*Phone: +7-4932-533784; fax: +7-4932- 336237; e-mail glp@isc-ras.ru.

ACKNOWLEDGMENT

This work was supported by ISTC (Project No. 0888) and the Russian Foundation of Basic Research N 09-03-00057.

REFERENCES

(1) Korolkovas, A. *Essentials of Medicinal Chemistry*, 2nd ed.; Wiley: New York, 1988; pp 699−716.

(2) Adsmond, D. A.; Grant, D. J. W. *J. Pharm. Sci.* **2001**, *90* (12), 2058–2077.

(3) Kelly, C. J.; Skakle, J. M. S.; Wardell, J. L.; Wardell, S. M. S. V.; Low, J. N.; Glidewell, C. *Acta Crystallogr.* **2002**, *B58*, 94–108.

(4) Parkin, A.; Collins, A.; Gilmore, C. J.; Wilson, C. C. *Acta Crystallogr.* **2008**, *B64*, 66–71.

(5) Allen, F. H. *Acta Crystallogr.* **2002**, *B58*, 380–388.

(6) Kalman, A; Czugler, M; Argay, G. *Acta Crystallogr.* **1981**, *B37*, 868–877.

(7) Senger, S.; Chan, C.; Convery, M. A.; Hubbard, J. A.; Shah, G. P.; Watson, N. S.; Young, R. J. *Bioorg. Med. Chem. Lett.* **2007**, *17*, 2931–2934.
(8) Bindal, R. D.; Golab, J. T.; Katzenellenbogen, J. A. *J. Am. Chem. Soc.* **1990**, *112*, 7861–7868.
(9) Higgs, T. C.; Parkin, A.; Parsons, S.; Tasker, P. A. *Acta Crystallogr.* **2002**, *E58*, o523–o525.
(10) Perlovich, G. L.; Strakhova, N. N.; Kazachenko, V. P.; Volkova, T. V.; Tkachev, V. V.; Schaper, K. J.; Raevsky, O. A. *Int. J. Pharm.* **2007**, *334*, 115–124.
(11) Perlovich, G. L.; Strakhova, N. N.; Kazachenko, V. P.; Volkova, T. V.; Tkachev, V. V.; Schaper, K. J.; Raevsky, O. A. *Int. J. Pharm.* **2008**, *349*, 300–313.
(12) Perlovich, G. L.; Tkachev, V. V.; Strakhova, N. N.; Kazachenko, V. P.; Volkova, T. V.; Surov, O. V.; Schaper, K. J.; Raevsky, O. A. *J. Pharm. Sci.* **2009**, *98*, 4738–4755.
(13) Guillory, J. K. *Polymorphism in Pharmaceutical Solids*; Brittain, H. G., Ed.; : Marcel Dekker Inc.: New York, 1999; pp 183−226.
(14) *CAD-4 Software*, Version 5.0; Enraf-Nonius: Delft, The Netherlands, 1989.
(15) Sheldrick, G. M. *SHELXL97 and SHELXS97*; University of Göttingen: Germany, 1997.
(16) Zielenkiewicz, W.; Perlovich, G.; Wszelaka-Rylik, M. *J. Therm. Anal. Calorim.* **1999**, *57*, 225–234.
(17) Cox, J. D.; Pilcher, G. *Thermochemistry of Organic and Organometallic Compounds*; , Academic Press: London, 1970.
(18) Chickos, J. S.; Acree, W. E., Jr. *J. Phys. Chem. Ref. Data* **2002**, *31* (2), 537–698.
(19) Dannenfelser, R.-M.; Yalkowsky, S. H. *J. Pharm. Sci.* **1999**, *88* (7), 722–724.
(20) Pascual-Ahuir, J. L.; Silla, E. *J. Comput. Chem.* **1990**, *11*, 1047.
(21) Raevsky, O. A.; Grigor'ev, V. J.; Trepalin S. V. HYBOT program package, Registration by Russian State Patent Agency N 990090 of 26.02.99.
(22) Etter, M. C. *Acc. Chem. Res.* **1990**, *23*, 120–126.
(23) Bernstein, J.; Davis, R. E.; Shimoni, L.; Chang, N.-L. *Angew. Chem., Int. Ed. Engl.* **1995**, *34* (15), 1555–1573.
(24) Mayo, S. L.; Olafson, B. D.; Goddard, W. A., III *J. Phys. Chem.* **1990**, *94*, 8897–8909.
(25) Perlovich, G. L.; Rodionov, S. V.; Bauer-Brandl, A. *Eur. J. Pharm. Sci.* **2005**, *24*, 25–33.
(26) Yalkowsky, S. H.; Valvani, S. C. *J. Pharm. Sci.* **1980**, *69*, 912–922.
(27) Li, Z. J.; Ojala, W. H.; Grant, D. J. W. *J. Pharm. Sci.* **2001**, *90*, 1523–1539.
(28) Gavezzotti, A.; Filippini, G. . Energetic aspects of crystal packing: Experiment and computer simulations. In *Theoretical Aspects and Computer Modeling of the Molecular Solid State*; Gavezzotti, A., Eds.; John Wiley & Sons: Chichester, 1997; Chapter 3, pp 61−97.